Journal of Materials Processing Tech. 275 (2020) 116350

Contents lists available at ScienceDirect

Journal of Materials Processing Tech.

journal homepage: www.elsevier.com/locate/jmatprotec

The influence of part asymmetry on the achievable forming height in multi-pass spinning

Iacopo M. Russo[a], Christopher J. Cleaver[a], Julian M. Allwood[a,*], Evripides G. Loukaides[b]

[a] Department of Engineering, University of Cambridge, Trumpington Street, Cambridge CB1 2PZ, UK
[b] Department of Mechanical Engineering, University of Bath, Claverton Down, Bath BA2 7AY, UK

ARTICLE INFO

Associate Editor: Zhenshan Cui

Keywords:
Metal spinning
Mandrel-free
Asymmetric shape
Forming height
Flexible manufacturing

ABSTRACT

Metal spinning is an incremental forming technique commonly employed in the production of hollow axisymmetric components. In recent years, asymmetric spinning processes have been developed to expand the range of component geometries achievable by the technique. However, most of these processes have employed a solid mandrel to set the target shape and provide internal support to the workpiece, thus requiring new tooling to be manufactured for every new part. Moreover, no studies have been performed on the link between the geometry of the target part and the achievable forming height. In this paper, the range of curvature in the target part's planform is used to quantify its degree of asymmetry, and the influence of this parameter on the formability of spun parts is investigated in a series of experimental trials. The hypothesis that the range of planform curvature predicts the likelihood of workpiece failure is tested. Methods to design the multi-pass toolpaths and the blanks required to spin both axisymmetric and asymmetric components without a mandrel are developed. The results show that increasing the degree of asymmetry of the target part only weakly influences the achievable forming height. This finding points to the potential of the technique to produce multiple geometries flexibly and to reduce the costs of prototyping and testing new sheet metal parts considerably.

1. Introduction

The stamping process is among the most popular techniques employed in the production of sheet metal parts today, but it requires expensive dedicated tooling and results in significant waste of material. As reported by Cooper et al. (2016), the material, engineering time and manual labour required to machine a die make up most of the costs of stamping at least up to a production volume of 1000 parts. Moreover, die making is the largest environmental cost component for low production volumes (up to 90 parts), while wasted sheet metal scrap becomes the largest for higher production volumes. Metal spinning is a nearly net-shape incremental forming technique used in the production of hollow axisymmetric components. Because only one die is required (the mandrel), the tooling costs and the set-up times are lower, thus making spinning advantageous for the small-to-medium volume production of sheet metal components. However, only axisymmetric geometries can be achieved by spinning, and a solid mandrel is still required for every new part geometry. This limits its advantages over stamping. If capable of producing multiple asymmetric parts flexibly, spinning could challenge stamping as the established technique to produce small batches of complex hollow sheet metal components. It could also provide a low-cost alternative to die-based techniques in the prototyping and initial development of new sheet metal parts and thus speed up innovation.

To overcome the inflexibility of metal spinning, Music and Allwood (2011b) built a machine that replaces the mandrel with three internal rollers (Fig. 1). This mandrel-free machine can potentially spin any rotationally symmetric and asymmetric part, but only the production of an axisymmetric component was demonstrated in the original work; more recently, Russo and Loukaides (2017) demonstrated the production of a shallow dish with a square-like planform (i.e. the component's outline as projected upon a plane normal to the central axis). In the present work, a new flexible toolpath generation algorithm for the trajectory of the rollers is developed, as well as a method to design appropriate blanks. Using these methods, this paper demonstrates the production of a range of asymmetric components with no dedicated tooling. The influence of the planform asymmetry on the achievable forming height is investigated experimentally.

In the next section, a review of the published literature on asymmetric spinning is presented. Then, in Section 3 the design of experiments is described together with the equipment and methods required to perform multi-pass asymmetric mandrel-free spinning. Section 4

* Corresponding author.
E-mail address: jma42@cam.ac.uk (J.M. Allwood).

https://doi.org/10.1016/j.jmatprotec.2019.116350
Received 30 January 2019; Received in revised form 19 June 2019; Accepted 28 July 2019
Available online 31 July 2019
0924-0136/

Nomenclature

b	blank perimeter line
Br, Bz	Blending Roller radial and axial coordinates (mm)
d	mandrel diameter (mm)
d_0	blank diameter (mm)
F	feed ratio (mm/rev)
F_z, F_r, F_{tot}	axial, radial and total roller force
κ	curvature (m^{-1})
L_0	initial flange length (mm)
L_f	final wall profile length or forming height (mm)
L_p	parameter to offset only a portion of the target part (mm)
m	coefficient in the offset function to define toolpass geometry
n	exponent in the offset function to define toolpass geometry
k	number of passes in a toolpath
n	normal vector
P	number of points in the toolpath per revolution
p	target part's planform line
ψ	degree of asymmetry
R	spindle revolution speed (rot/min)
r_{rol}	roller radius (mm)
r_n	roller nose radius (mm)
S	spinning ratio
t_0	blank thickness (mm)
v	roller feed rate (mm/min)
Wr, Wz	Working Roller radial and axial coordinates (mm)

presents the results of the trials investigating the influence of asymmetry on formability, while Section 5 discusses the results with a more detailed analysis of tool forces, thinning and shape error.

2. Literature review

In this section, a review of the relevant literature will be presented. A general description of the spinning process and the modes of workpiece failure will be given first; then, approaches to asymmetric spinning will be reviewed, highlighting the differences with axisymmetric spinning.

Fig. 2 presents a schematic of the metal spinning process, including definitions of the process parameters and common part geometries. As reviewed by Music et al. (2010), two variations of spinning exist. In shear spinning, the diameter of the final part remains equal to that of the starting blank, while the thickness reduces according to the sine law. Forming occurs in a single roller pass, and the most important process parameter is the feed ratio F, defined as the ratio between the roller feed v and the spindle revolution speed R:

$$F = \frac{v}{R} \tag{1}$$

Only conical or hemispherical parts can be produced with this technique, as shown in Fig. 2(c); vertical or re-entrant walls cannot be achieved, because the part wall would break. In conventional spinning, multiple roller passes are required to achieve the final shape; the most important process parameter, together with the feed ratio F, is the multi-pass trajectory of the roller, commonly called the toolpath. When performed by skilled operators, the thickness of the final part in conventional spinning remains more or less equal to that of the starting blank, while the diameter reduces. Parts with vertical walls as well as re-entrant walls can be produced, as shown by Fig. 2(d).

The achievable forming height, as defined in Fig. 2(d), and the speed of the spinning process are limited by two fundamental failure modes: tearing and wrinkling. Xia et al. (2005) developed a spinning process window with two fundamental parameters: the feed ratio F, defined as above, and the spinning ratio S, defined as the ratio of blank diameter d_0 to mandrel diameter d:

$$S = \frac{d_0}{d} \tag{2}$$

They showed that any increase in feed ratio F is limited by the increasing likelihood of wrinkling; any increase in spinning ratio S is limited by the increasing likelihood of circumferential tearing. This is confirmed in many studies linking feed ratio to wrinkling and spinning ratio to tearing, including Watson and Long (2014) and Hayama et al. (1970). Lange (1985) reported that a higher sheet thickness allows higher spinning ratios to be achieved for a given mandrel size and roller nose size. Common values for S lie between 1.2 and 1.6, but values as high as 2.4 have been achieved by Ahmed et al. (2015) using a very large roller nose size and stabilising the blank edge with a blank holder.

Both shear and conventional spinning require a mandrel to set the final geometry of the component and provide internal support to the workpiece during the process. This increases the costs and the lead times for producing new parts. To realise a more flexible spinning process, a few researchers have attempted to develop mandrel-free versions of spinning. Shima et al. (1997) replaced the mandrel with one internal roller, which moved together with the outside roller to form conical components with reduced thickness. The angle and wall thickness were controlled via the feed ratio F alone. Kawai et al. (2001) used a simple cylindrical mandrel with no blank holders nor internal rollers to spin a variety of conical and hemispherical parts. Both these works present equipment built to perform shear spinning; the only mandrel-free machine built to perform conventional multi-pass spinning is that by Music and Allwood (2011a), whose schematic design is presented in Fig. 3(a). In this configuration, the mandrel is replaced by three internal rollers: a blending roller usually sitting at the corner of the target part, and two rollers supporting the flange of the workpiece in the later stage of the process. Toolpaths for all rollers employed in the process must be designed to spin a component, although not all internal rollers are necessary for all parts. With this configuration, axisymmetric parts with straight and re-entrant walls have been produced, as shown in Fig. 3(b). More recently, Russo and Loukaides (2017) used the equipment to spin a dish with a square-like cross section, as shown in Fig. 3(c).

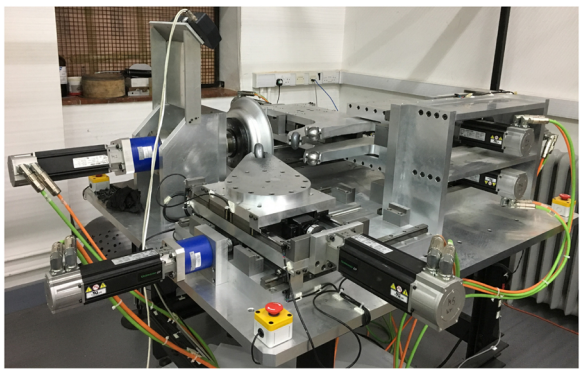

Fig. 1. A photograph of the mandrel-free spinning machine designed and built by Music and Allwood (2011b) at the University of Cambridge.

2.1. Asymmetric spun parts

Although spinning traditionally produces axisymmetric components, in the last thirty years researchers have attempted to expand its capabilities to produce more complex parts. Here, the approaches taken to date to spin parts with an asymmetric planform will be reviewed.

Most researchers have employed one-pass shear spinning with a

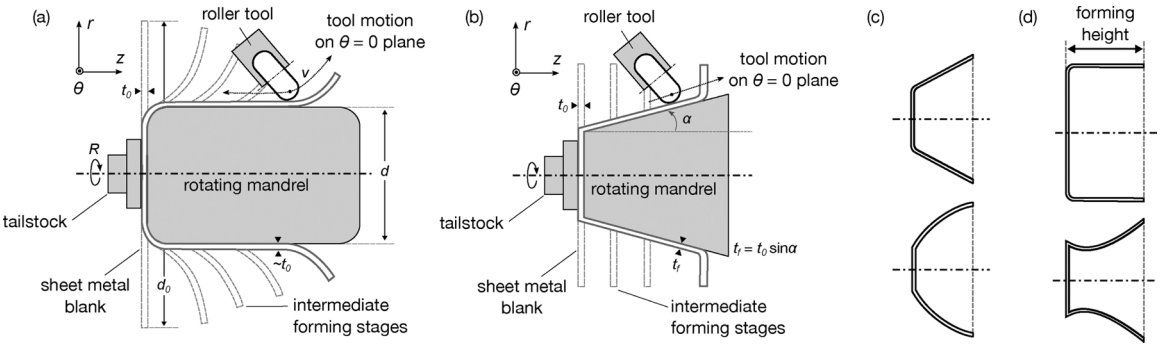

Fig. 2. (a) Conventional spinning, showing the relevant process parameters; (b) shear spinning and the sine law; (c) axisymmetric part geometries achievable by shear and conventional spinning; (d) geometries achievable by conventional spinning only, and the definition of forming height.

mandrel to make asymmetric components. Two control approaches have been taken to achieve this: position and force control. The first to make an asymmetric component by position-controlled spinning were Amano and Tamura (1984), who achieved an elliptical cone by employing a radially offset roller on a modified spinning lathe. Then, Gao et al. (1999) used a similar approach but offset the mandrel while keeping roller fixed radially. They succeeded in producing a 10-mm deep elliptical cup with a straight wall in one pass as well as a deeper elliptical cone. Shimizu (2010) succeeded in forming parts shaped as an elliptical cone and as a truncated pyramid by synchronising the mandrel motion, the mandrel feed and the roller feed by pulse control. The advantage of this approach is that only the mandrel and the software code must be changed to spin a different geometry, rather than the whole equipment. Xia et al. (2010) developed a spinning method based on a profiling mandrel and then used it to make conical products in one pass with a variety of cross-sections, including triangular, square and pentagonal. The profiling mandrel was developed solving a geometrical model analytically and the setup showed very good tolerance. However, this set-up is also inflexible: conical parts can be formed and two new mandrels must be manufactured for every geometry.

Force control in asymmetric spinning was proposed by Awiszus and Meyer (2005). They used a pair of spring-controlled rollers to make a part with a tripode cross-section. Although they succeeded in producing the part, they reported significant variations in thickness both along the radial and circumferential direction. This was addressed in later publications e.g. by Härtel and Laue (2016) but their set-up was changed to have motion-controlled rollers instead. A hybrid force/position-control approach was taken by Arai (2005): the roller is position-controlled to move at a constant velocity parallel to the mandrel surface, and is made to apply a constant pushing force normal to the surface. A truncated pyramid and a cone with an eccentric cross-section were successfully spun using this method. Thus, force control approaches have been successful in achieving conical components, but are only applicable to shear spinning. An attempt to produce a conical component with a square cross section without a mandrel was made by Jia et al. (2015) by employing a square clamping shaft (or headstock). Although forming was performed in the absence of a mandrel, because the only internal support provided to the workpiece is at the base, this set-up requires a different clamping shaft for every shape. Sugita and Arai (2015) were the first to perform multi-pass spinning on a part with an asymmetric planform and vertical walls. They developed a synchronous multi-pass spinning method which could apply to both axisymmetric and asymmetric planforms and applied it to a circular and a square cup. Their setup employed a mandrel. They found that a lower height could be achieved in an asymmetric component than in an axisymmetric one (the max height for the square cup was 40 mm, compared to 65 mm for the circular one). Finally, an attempt to perform multi-pass spinning without a mandrel on an asymmetric part was made more recently by Russo and Loukaides (2017), who developed a toolpath generation method to spin a square dish with vertical walls. However, this part had a limited spinning ratio S of 1.15, and the ability to produce components with greater S has not been explored yet.

2.2. Differences between axisymmetric and asymmetric spinning

The geometry and mechanics of asymmetric spinning are significantly more complicated than those of axisymmetric spinning. In this section, three aspects of asymmetric spinning will be reviewed: the roller–workpiece contact, the design of blanks, and the thinning in the part.

While in axisymmetric spinning the point of contact between the workpiece and the tool always lies in the plane of motion of the roller, in asymmetric spinning this is no longer the case. Methods to synchronise the motion of the roller with the rotation of the spindle and position it at the correct radial position are necessary. Three approaches to solving this problem are found in the literature. The first approach, used by Amano and Tamura (1984) and by Gao et al. (1999), is to make the roller follow the rotation of the mandrel using physical

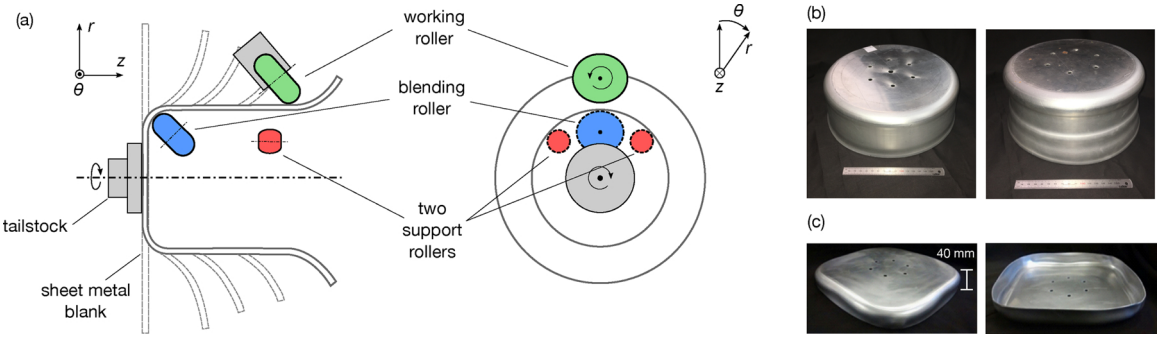

Fig. 3. (a) A schematic design of the flexible spinning machine built by Music and Allwood (2011a); (b) axisymmetric parts with straight and re-entrant wall profiles made with this process; (c) a shallow square-like part made by Russo and Loukaides (2017) with this process.

mechanisms. The former used a mechanism of cams and links to guarantee the correct oscillatory motion of the roller; the latter keep the point of contact between roller and mandrel fixed, while the offset of the mandrel from the central axis changes thanks to a movable revolving drum. In principle, this method is applicable to any mandrel geometry, but the roller must always adhere to the mandrel and therefore only one-pass shear spinning is possible. Xia et al. (2010) used a profiling mandrel. With the use of gears, this can replicate the motion on the main mandrel and synchronise the roller radial motion. This approach is accurate but presents several disadvantages: it only works with mandrel-based spinning, two mandrels must be manufactured for every new shape, and only one-pass spinning can be performed. Sugita and Arai (2015) used force control to obtain a profile of the mandrel. At the start of the process, the roller is made to run along the mandrel to obtain a profile, which is then fed to the synchronous multi-pass algorithm that generates the correct trajectory for the roller. This method circumvents the need for a complicated geometric model of a non-spherical roller and an asymmetric mandrel, but requires taking a profile of every new shape and is not applicable to mandrel-free machines. Thus, no general approach applicable *a priori* to any target geometry or without employing a mandrel has been developed so far.

The design of the blank for asymmetric parts influences the forming conditions and the material efficiency of the process, but the issue has been given little attention in the literature. None of the works mentioned above in shear spinning developed an explicit method for blank design. Arai (2005), Awiszus and Meyer (2005) and Awiszus and Härtel (2011) used circular blanks. Amano and Tamura (1984) and Gao et al. (1999) do not clarify whether they used circular or elliptical blanks, and do not discuss the issue. Shimizu (2010) and Xia et al. (2013) used blanks with the same shape as the target (elliptical and triangular respectively) but do not discuss how the blank geometry was calculated. Finally, Cheng et al. (2013) designed pentagonal blanks starting from the target part and using the software Dynaform but gave no details on the parameters selected. In multi-pass spinning, Sugita and Arai (2015) used a circular blank and adapted the toolpath to interpolate between the planform of the target part and the blank. This led to significant extra material leftover along the corners at the end of the process. It can be concluded that a consistent method to design blanks targeted for asymmetric shapes has not been developed yet.

Finally, the pattern of thinning in the part is expected to be different in axisymmetric and asymmetric spinning, since the local curvature around the workpiece changes in asymmetric parts. Shimizu (2010) measured the strain distribution along radial profiles of the part after one-pass elliptical cone spinning. They found that radial thickness profiles are similar in the circular and elliptical cones, but the maximum thinning is higher along the long axis of the ellipse (where the local curvature is higher) rather than the short axis. This was the case for the elliptical cone made by Gao et al. (1999), too. Cheng et al. (2011) numerically investigated the effect of part asymmetry on the distribution of thickness in a square-like part. Similar to axisymmetric spinning, they found that thinning occurs at the junction between the bottom and the wall of the workpiece, while thickening occurs at the edge. Contrary to Shimizu (2010) and Gao et al. (1999), they found the highest thinning to happen near the area of the workpiece with lower local curvature. Sugita and Arai (2015) found that the thickness of square cups increased by up to 80% in the corners compared to the thickness in the sides. Conversely, Awiszus and Meyer (2005) found that the thickness of Reuleaux triangle-shaped workpieces decreased significantly in the corners compared to the sides. In conclusion, there is limited knowledge on how asymmetry affects thinning, and authors have found opposite trends in the relationship between thinning and local curvature for different target geometries.

2.3. The scope of the present work

This review of asymmetric spinning research reveals that many complex parts have been produced, including elliptical, triangular, square, pentagonal, tripode- and pagoda-shaped planforms. However, the range of wall profiles has been very limited; in fact, excluding the work of Sugita and Arai (2015), all parts mentioned have been made by one-pass shear spinning and therefore had a conical wall profile with reduced thickness. Moreover, all the components made so far have required part-specific tooling (the mandrel or a special clamping shaft) and no general methods have been developed to approach the problems of roller–workpiece contact and blank design. Finally, the influence of asymmetry over thinning and failure remains unclear.

Therefore, the first aim of this paper is to establish a general methodology to spin a variety of axisymmetric and asymmetric parts with no dedicated tooling. The second aim is to use this methodology to investigate the influence of the planform asymmetry on the mechanics and on the achievable forming height in spinning. A measure based on the planform curvature is proposed quantify the degree of asymmetry of a shape and to predict, for a given spinning set-up, an increase in the chances of workpiece failure. Thus, this work aims to develop a better understanding of what features may reduce the failure-free process window of asymmetric spinning, so as to aid process selection when designing a new sheet metal component.

3. Methodology: investigating the influence of asymmetry on formability

In axisymmetric spinning, the target part's planform is a circle; therefore, there is no circumferential variation in curvature and deformation occurs homogeneously. In asymmetric spinning, the planform deviates from axisymmetry as the local curvature changes around the perimeter. The hypothesis is made that the greater the deviation, the greater the reduction in the achievable forming height in spinning. To test this hypothesis, a quantitative definition of asymmetry based on planform curvature is developed in the next section, and a set of target component geometries are selected to perform experimental trials. The spinning equipment used to perform the experiments is then described, followed by the methods developed to generate toolpaths and blanks for the mandrel-free asymmetric spinning process.

3.1. Design of experiments

To assess the formability of spun parts, the spinning ratio S is employed, as defined previously in Eq. (2). The spinning ratio is a normalised measure of the target forming height (or, more generally, of the final wall profile length) of a spun component, so it is suitable to assess formability. However, it can only be applied to axisymmetric parts. In deep drawing, when asymmetric parts must be drawn, a drawing ratio can still be defined by using equivalent diameters (Lange, 1985). The

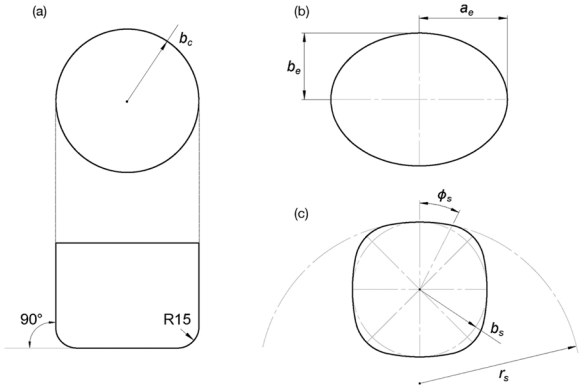

Fig. 4. Planforms of the component geometries investigated in this study, showing their parameterisation: (a) circular part, also showing the target wall profile common to all parts; (b) elliptical part; (c) square part.

Table 1
Dimensions and geometrical properties of five target part's planforms chosen to investigate the influence of asymmetry on formability.

Shape	Dimensions (mm)			κ_{max} (m^{-1})	κ_{min} (m^{-1})	ψ
Cr	b_c = 144.3			6.93	6.93	0.0
El1	b_e = 130.5	a_e = 159.5		9.37	5.13	0.6
El2	b_e = 125.0	a_e = 166.5		10.66	4.51	0.9
Sq1	b_s = 137.0	r_s = 328.0	ϕ_s = 27°	12.17	3.05	1.3
Sq2	b_s = 136.0	r_s = 360.0	ϕ_s = 30°	14.25	2.78	1.7

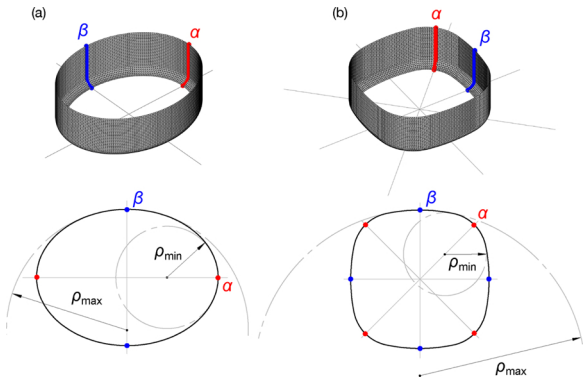

Fig. 5. Definition of the α-cut and the β-cut for (a) elliptical target parts and (b) square target parts. The profiles are obtained by cutting the target part with a vertical plane at the points of κ_{max} and κ_{min} in the planform.

equivalent diameter d' of a non-axisymmetric planar shape is the diameter of the circle with the same area as the shape. Hence, an equivalent spinning ratio can be defined as:

$$S' = \frac{d_0'}{d'} = \sqrt{\frac{A_0}{A}} \tag{3}$$

where d_0', A_0 and d', A are the equivalent diameters and areas of the asymmetric blank shape and of the target part's planform respectively. Therefore, S' can be calculated consistently for parts with any planform geometry and will be used as a measure of formability in the experimental trials.

To test the hypothesis that the deviation from axisymmetry predicts the likelihood of workpiece failure, a measure is developed to quantify this deviation based on the range of planform curvature κ. The measure ψ is defined as follows:

$$\psi = \frac{d'}{2}(\kappa_{max} - \kappa_{min}) \tag{4}$$

where κ_{max} and κ_{max} are the max and min local curvatures found around the planar shape of the planform. Thus, ψ is defined as the normalised degree of asymmetry of a planar shape based on the variation of the local curvature. It is generally applicable to all closed planar shapes, and can account for features such as straight lines, discontinuous changes in the local curvature (e.g. in corners of a certain radius) and curvatures of opposite sign (i.e. concave sides). The equivalent diameter d' is used to normalise ψ with respect to the absolute size of the target part, in the same way as the equivalent spinning ratio S'.

To evaluate the influence of asymmetry on the formability, five geometries with increasing ψ are selected: a circular part, two elliptical and two square parts. The planform of these three geometries is shown in Fig. 4. The circular and elliptical planforms are parameterised with a radius b_c for the circle and with major and minor axes b_e and a_e for the ellipse. The square planform is parameterised using two circle arcs: one from a circle with a large radius for the side, and one from a circle with small radius for the corner; this shape is fully defined by the radius b_s of the inscribed circle, the radius r_s of the large circle arc, and an angle ϕ_s over which this arc extends. Table 1 lists the values of the parameters used to define the five component geometries, and it gives the values of κ_{max}, κ_{min}, and ψ. All target geometries share the same wall profile: a vertical wall (90° to the horizontal) with a 15 mm fillet radius, as shown in Fig. 4(a). A 5 by 5 matrix of experimental trials is planned: for each target geometry, 5 trials are performed with the spinning ratio S' starting at 1.25 and increasing by 0.05, until failure is encountered. All geometries are designed to have the same planform area A, so that, for a given value of S', the initial flange length (i.e. the section of the workpiece that undergoes deformation) is the same: $L_0 = (d_0' - d')/2$. Thus, the achieved forming heights L_f can be directly compared.

To simplify the analysis of the results, the points of max and min curvature κ_{max} and κ_{min} around the perimeter of the target geometries are defined as α and β. Fig. 5 shows the osculating circles constructed at these two key points in the perimeter for the elliptical and square part. The relationship between the radii of curvature ρ and the curvature κ is defined as:

$$\kappa_{max} = \frac{1}{\rho_{min}}, \qquad \kappa_{min} = \frac{1}{\rho_{max}} \tag{5}$$

If the target part is cut with a vertical plane at these points in the planform, wall profile cuts are obtained, as shown in Fig. 5. Along these cuts, the normals to the target part's surface are aligned with lines passing through the part's centre. Measurements of roller forces, workpiece thickness and shape will be made along these key profiles to gain an insight into the mechanics of asymmetric mandrel-free spinning.

3.2. Spinning equipment

All experimental trials are performed with the mandrel-free spinning machine built by Music and Allwood (2011a) at the University of Cambridge. The experimental set-up is shown in Fig. 6. Two rollers are used: the Working Roller (WRol), which corresponds to the main roller in conventional spinning; and the Blending Roller (BRol), which is

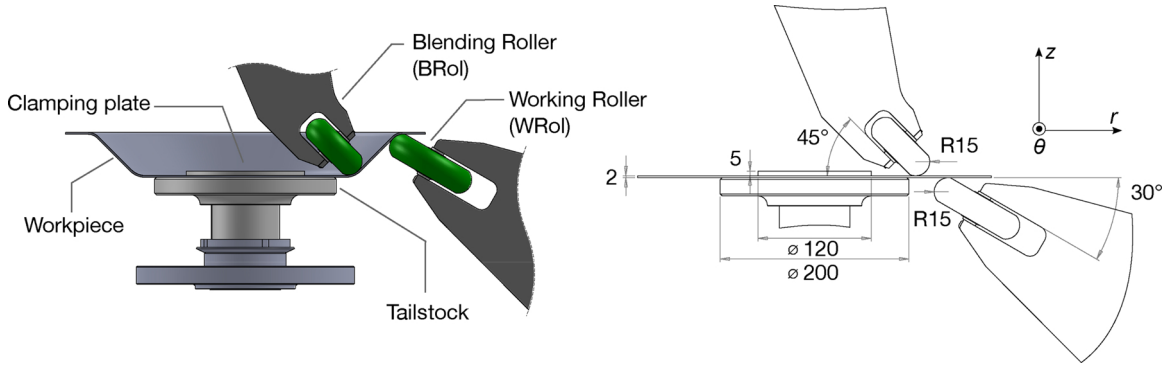

Fig. 6. The set-up of the mandrel-free spinning machine used in this study, with the key dimensions of its components.

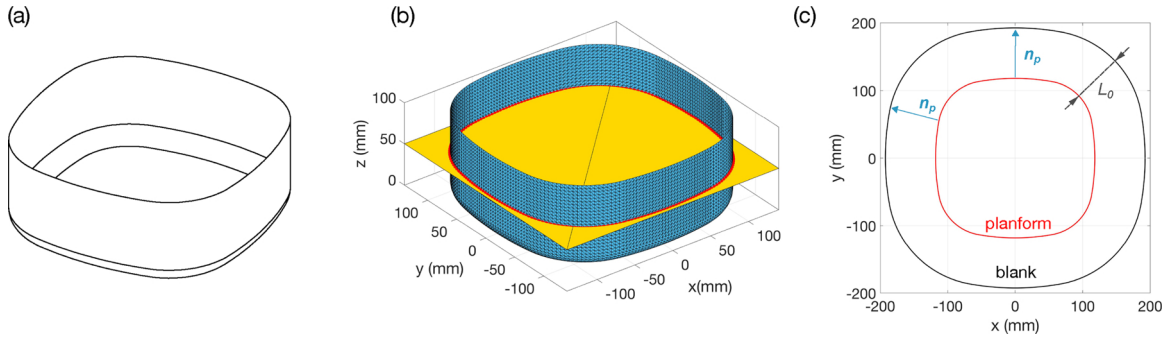

Fig. 7. The blank design method used in this study: (a) the CAD model of the target part is obtained, in this case a square part; (b) the planform is obtained by slicing the target part with a horizontal plane; (c) material is added to obtain the initial flange length L_0 at all points around the perimeter.

positioned at the filleted corner of the would-be mandrel.

All trials are performed on blanks made of Al 1050-H14 and 2 mm thickness, cut from rolled sheet. The rolling direction is aligned consistently for each target geometry. The sheet is clamped to the tailstock using a small circular clamping plate, as shown by Fig. 6. The spindle rotational speed R is set as 100 RPM for the axisymmetric trials and 15–20 RPM for the asymmetric trials. The WRol and BRol move on a plane in the radial (r) and axial (z) directions and the coordinates (Wr, Wz) and (Br, Bz) on the $\theta = 0$ plane refer to the nose centre. Three quantities are measured during or after the trials: roller forces in the r and z-direction; workpiece wall profile shape; and thinning along radial and circumferential cuts in the workpiece. Details for the motion control system and for measurements taken are given in Appendix A.

To perform the planned matrix of experimental trials with the mandrel-free spinning equipment described, methods to design

Table 2
Toolpath and toolpass parameters editable by the user in the developed toolpath generation algorithm.

For the full toolpath	
k	Number of toolpasses
P	Number of points per mandrel revolution
F	Feed ratio (mm/rev) along the current toolpass slope
For each toolpass	
L	Pass length (mm)
n, m	Exponent and coefficient in the pass geometry function
L_p	Distance along the mandrel's meridian where offset should start (mm)

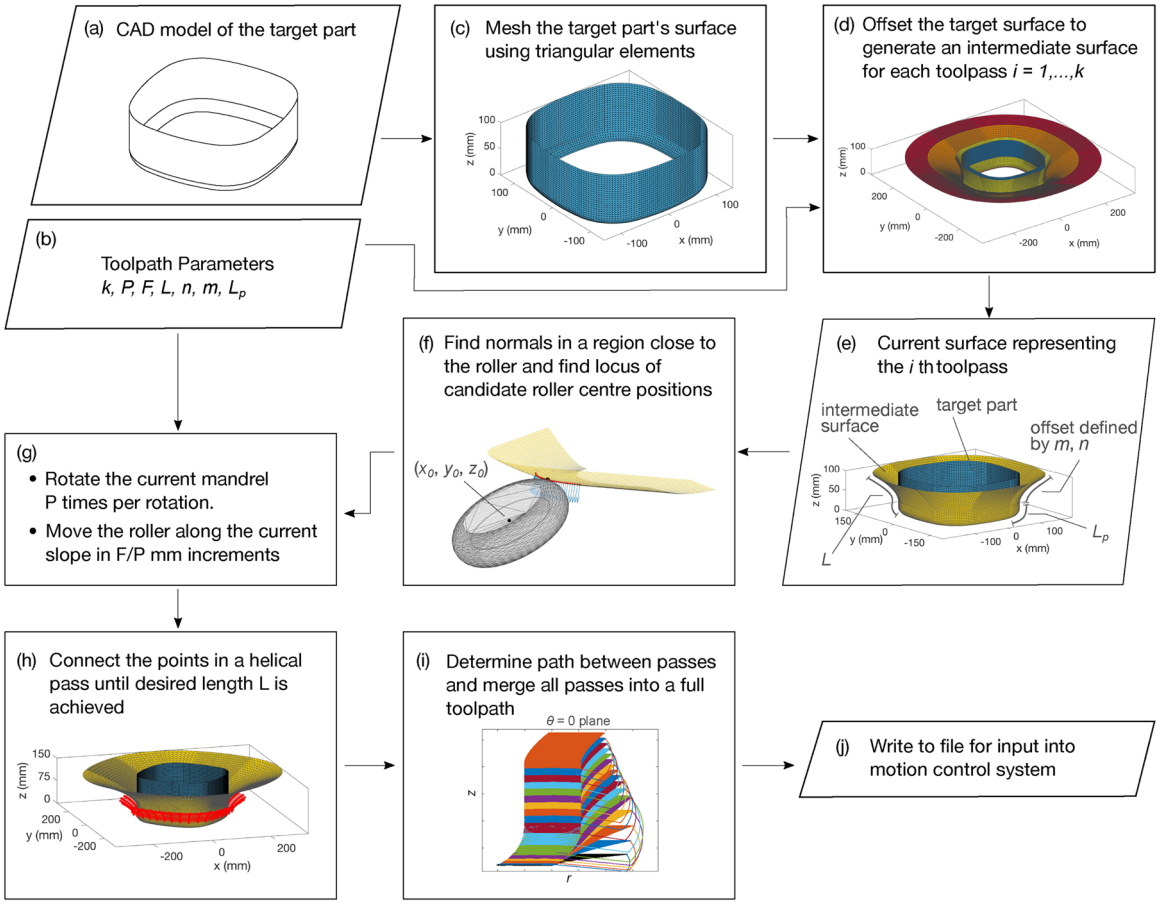

Fig. 8. Flowchart of the steps involved in the toolpath generation algorithm. Parallelograms indicate inputs and outputs, while rectangles indicate processes.

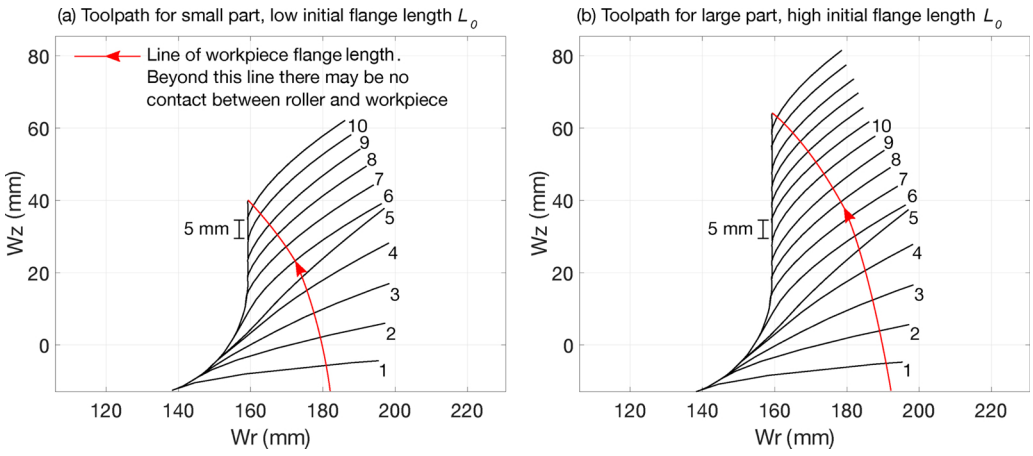

Fig. 9. The 2D profile of the WRol toolpath used in this study, showing 5 toolpasses in rotational sequence, followed by $(k - 5)$ toolpasses advancing 5 mm on the mandrel each in a translational sequence. (a) Shows the toolpath used for a small part, which requires fewer toolpasses to complete, while (b) shows the toolpath used for a large part, which requires more passes to complete. In both cases, the geometry and sequence of passes is the same.

Table 3
Values selected for the parameters of the toolpath used in this study, whose design is graphically shown in Fig. 9.

For the full toolpath										
k	15 or more									
P	36 for asymmetric shapes; 1 for the axisymmetric shape									
F	1 mm/rev									
For each toolpass										
Pass number i	1	2	3	4	5	6	7	8	9	10 onward
n	1.8	1.8	1.6	1.5	1.3	1.7	1.7	1.7	1.7	1.8
m	1.1	0.27	0.24	0.21	0.32	0.075	0.071	0.067	0.064	0.043
L_p (mm)	7	8.6	10.1	11.8	13.5	18.5	23.5	28.5	33.5	$L_p(i-1)+5$

toolpaths and blanks for both axisymmetric and asymmetric parts are required. The method used to generate the toolpath must account for the roller–workpiece contact occurring outside of the plane of the rollers. Both the toolpath and the blank design methods must be generally applicable to both axisymmetric and asymmetric parts. The next two sections describe the solutions developed to meet these requirements.

3.3. Blank design

The method used to design the contour of the starting blank for each axisymmetric and asymmetric shape spun is shown in Fig. 7. A CAD model of the part is obtained and the outer surface is meshed using triangular elements. Then, a plane is made to slice the mesh perpendicularly to the central axis of the part to obtain the planform. The resulting 2D curve is shown in red in Fig. 7(c). Then, material is equally added around the perimeter according to the equation:

$$\mathbf{b} = \mathbf{p} + L_0 \mathbf{n_p} \tag{6}$$

where $\mathbf{b}$ is the blank contour, $\mathbf{p}$ is the target part's planform, L_0 is the amount of material in mm to be added and $\mathbf{n_p}$ is the vector normal to $\mathbf{p}$ at every point. L_0 is the initial flange length: this parameter will be used in the toolpath generation to set the length L of the first toolpass. The blank generation method is generally applicable to any target part with vertical walls defined by a planform with continuous curvature; it can be easily adapted to other wall profiles by slicing the part at the top of the part and adjusting L_0 to the length of the part's wall profile.

3.4. Toolpath generation and design

To generate toolpaths for both the working roller and blending roller, an algorithm applicable to all target geometries is developed. The steps followed by the algorithm are presented in Fig. 8, while the parameters used to generate the toolpath and editable by the user are listed in Table 2. A CAD model of the part, together with the toolpath parameters, are the inputs to the toolpath generation algorithm. Firstly, the outer surface of the part is meshed using triangular elements. For each toolpass, the surface of the target part is then offset according to

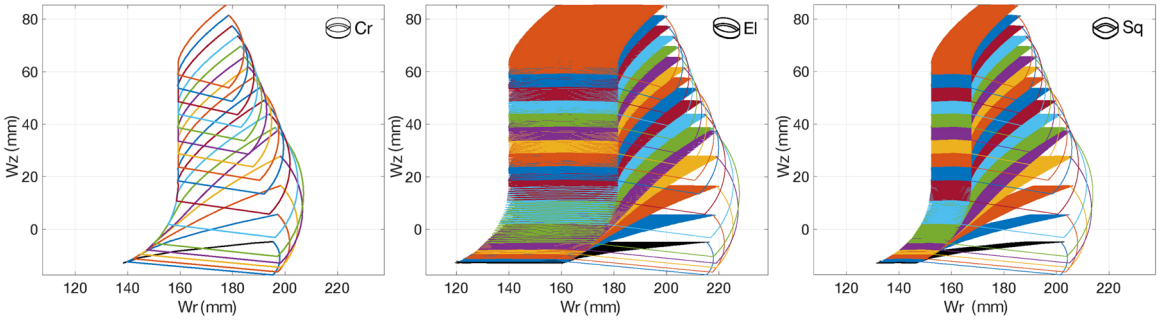

Fig. 10. The full paths output by the toolpath generation algorithm for a circular part (Cr), an elliptical part (El) and a square part (Sq). The profile of the toolpath as shown in Fig. 9 is the same for all three parts.

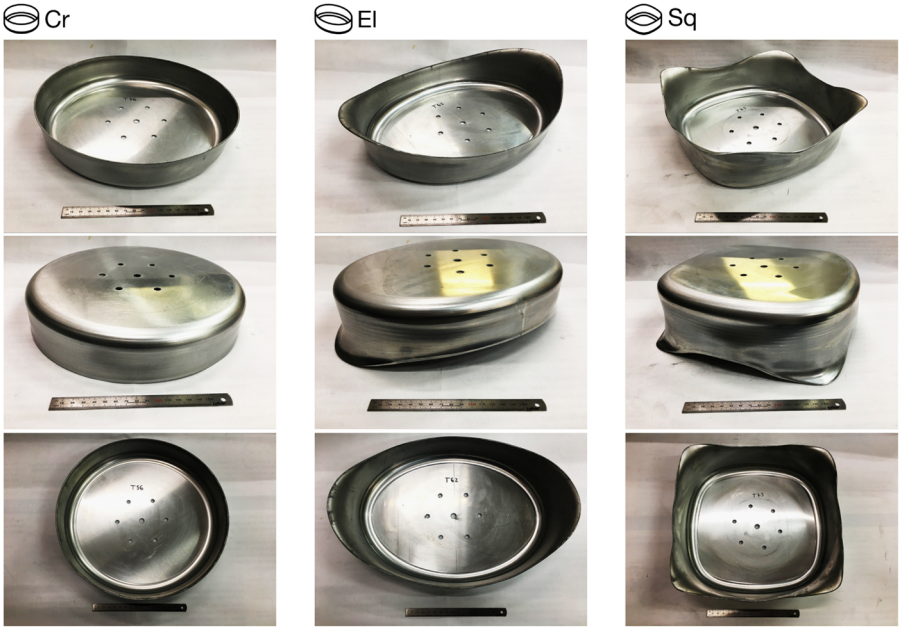

Fig. 11. A circular (Cr), elliptical (El) and square (Sq) part photographed from different perspectives. Earing can be observed in the two asymmetric shapes (El and Sq) along the areas of higher planform curvature κ.

the parameters m, n and L_p. Each intermediate, offset mandrel surface corresponds to an individual toolpass of an axisymmetric spinning process, as shown by Fig. 8(e). Following the definitions of Hayama et al. (1970) and Sugita and Arai (2015), both rotational and translational toolpasses can be designed in this way. The parameters m, n define the geometry (slope and concavity) of the rotational pass, while the parameter L_p allows offsetting only a selected portion of the target surface, so that toolpasses can translate forward on the target part like in translational toolpaths.

Once obtained, the intermediate mandrel surface is made to rotate P times and the WRol is made to move forward by F/P distance increments, so that a distance equal to F has been covered in one revolution. At every point, the correct position of the roller centre (x_0, y_0, z_0) is calculated by choosing among a set of candidate positions at each axial position z_0. Details for the calculation are given in Appendix B. The positions are connected to create a helical pass on the intermediate mandrel surface, as shown in Fig. 8(h), until the prescribed pass length L is reached. The helical pass in (x, y, z) coordinates is then translated to cylindrical coordinates (r, z, θ). The path between successive passes is designed as a circle arc and the whole toolpath is merged together. The process is the same for the BRol, but the z_0 coordinate of the contact point is chosen arbitrarily at a suitable point; this is because the mandrel surface at the part's filleted corner is convex and has the same radius as the BRol nose radius, so that the roller–workpiece contact may occur at multiple points simultaneously. The BRol is made to follow the same trajectory at the corner of the target part, i.e. it has $F = 0$ mm/rev. However, because the contact point is fixed and the slope of the wall changes, oscillatory motion in the z-direction up to 1 mm in amplitude is observed.

Having explained the method to generate toolpaths, the determination of suitable parameters for the toolpath design will now be discussed. The WRol toolpath profile designed to spin all parts (both axisymmetric and asymmetric) in this study is shown in Fig. 9 and the values for its parameters are given in Table 3. To determine these values, we used the results of the study carried out by Sugita and Arai (2015), which found that translational toolpaths with low distance between toolpasses achieve the highest forming height, and the study by Hayama et al. (1970), which found that concave passes give the highest spinning ratio. Starting from these assumptions, we performed a few exploratory trials on both axisymmetric and asymmetric parts, to

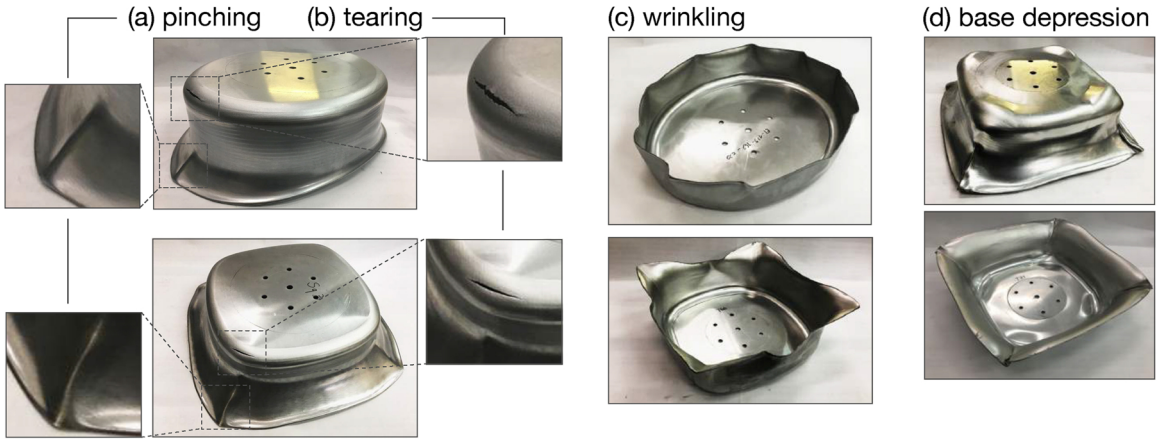

Fig. 12. Failure modes encountered in the experimental trials: (a) pinching, (b) tearing, (c) wrinkling and (d) base depression. Wrinkling and tearing are commonly encountered in conventional spinning, but pinching and base depression are specific to asymmetric mandrel-free spinning.

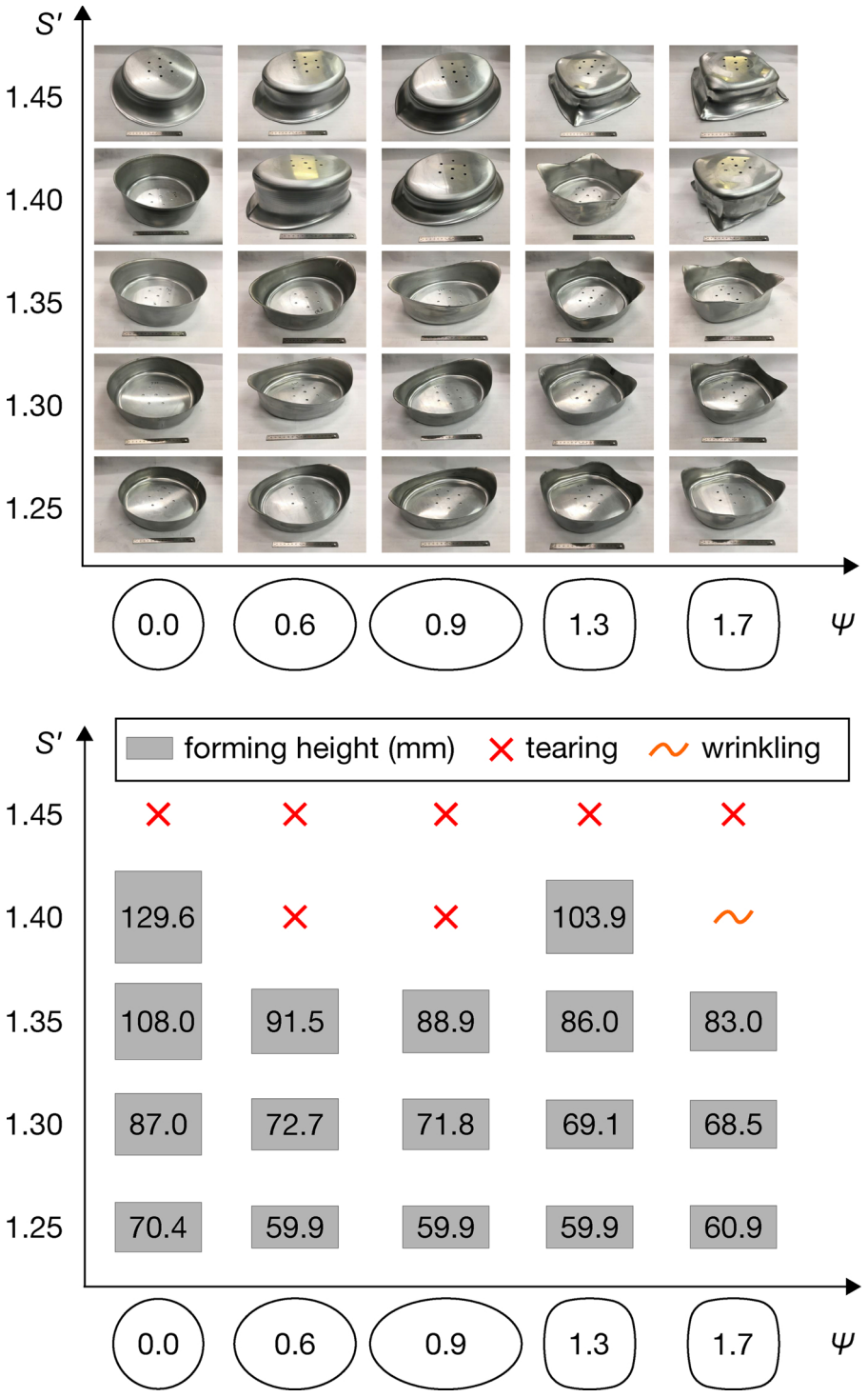

Fig. 13. The results of the 5 by 5 matrix of trials performed to investigate the influence of asymmetry on formability in asymmetric mandrel-free spinning. In the top graph, the cups facing up are successful, while the cups facing down have cracked or wrinkled.

find parameters that would be suitable for all parts. Thus, the feed ratio F is set as 1 mm/rev in the direction of roller motion. The parameters n and m are chosen so that all toolpasses have concave or nearly linear geometry. Only forward passes are used. A rotational toolpath sequence is selected for the first 5 passes, until the workpiece flange forms an angle of 45° with the r-axis. Then, the sequence is translational in the following passes: L_p is increased by 5 mm in each pass, and the workpiece flange is kept at the same angle of 35–40° with the r-axis (depending on the length of the pass). The value for L_p was chosen by trial and error during the exploratory trials. The length L of the first pass is set equal to L_0; each subsequent pass increases in length by 1–5 mm to account for thinning in the workpiece and consequent lengthening of the flange. Fig. 9 shows that a lower number of passes k is needed to achieve a vertical wall for parts with low L_0; a higher k is required for parts with high L_0. As will be shown, asymmetric parts also show earing, so during one rotation the WRol may lose contact with the workpiece where the forming height is lower.

The flexibility of the toolpath generation algorithm is demonstrated by Fig. 10. The WRol toolpath profile that was shown in Fig. 9 is now presented in full for the axisymmetric (or circular, Cr), elliptical (El)

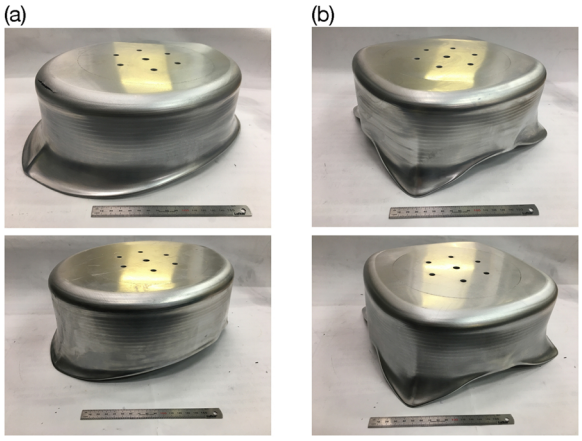

Fig. 14. (a) Elliptical parts with $\psi = 0.6$ and $S' = 1.40$; (b) Square parts with $\psi = 1.3$ and $S' = 1.40$. In the top pictures, the rolling direction is aligned with the α-cut, in the bottom with the β-cut.

and square (Sq) target parts. The user only needs to specify the toolpath parameters and the target component geometry; the toolpath generation algorithm will output the correct trajectory for the rollers to follow. This will account for roller–workpiece contact occurring outside of the plane of the rollers, and will work for axisymmetric and asymmetric shapes alike.

4. Results

With the equipment and methods described in the previous section, the matrix of experimental trials to investigate the influence of planform asymmetry on formability can be performed. In this section, the general features of asymmetric spun parts and the encountered failure modes will be described first; then, the results of the matrix of trials will be shown and discussed.

Photographs of successful production of a circular, square and elliptical parts are presented in Fig. 11. They show that the achieved forming height in asymmetric parts is uneven: earing is observed in proximity of the α-cut, i.e. in areas of higher κ in the planform. This effect can be explained by volume constancy considerations. For all target geometries, the starting blank is designed by adding material equally around the planform. In areas where the local radius of curvature ρ is smaller (and the curvature κ is higher), material must accumulate either in the radial or thickness direction; therefore, the accumulation can be relieved either by thickening or by earing of the workpiece in those areas. In the present experimental conditions, earing dominates and the parts exhibit uneven forming height. This does not constitute workpiece failure, since the parts can always be trimmed after spinning to achieve a constant height around the part.

The failure modes encountered in the experimental trials are illustrated in Fig. 12. In addition to tearing and wrinkling, which are commonly encountered in conventional spinning, asymmetric parts may sometimes exhibit pinching along the wall, at the point of highest κ in the planform. This can be described as a stiffened, folded section of the workpiece flange, as shown by Fig. 12(a). As the WRol keeps passing over these stiffened sections, the workpiece base tends to depress. This is especially evident in square parts, as shown in the photographs in Fig. 12(d). Tearing is nearly always observed to occur at the filleted corner of the part at the point of highest κ in the planform (the α point).

Having described the earing effect and the failure modes, the results of the 5 by 5 matrix of trials can now be discussed. Fig. 13 shows two graphs arranging the five selected geometries in order of increasing ψ on the x-axis, while the increasing S' is displayed on the y-axis. Because both the design of the blank and the toolpath parameters have an influence on the achievable S', the values for all process variables are kept constant across experiments: the toolpath shown in Fig. 9 with $F = 1$ mm/rev is used and blanks are designed in the same way for all parts, as explained in Section 3.3. Thus, all parts on these graphs can be directly compared. The highest spinning ratio achieved without failure for all geometries is 1.35. At $S' = 1.40$, only the circular part and the square with lower ψ are formed without failure; the two elliptical parts fail by tearing, while the square with higher ψ fails by wrinkling. At $S' = 1.45$, all parts fail by tearing at the filleted corner (where the BRol is positioned during the trial); the only exception is the square part with higher ψ, which fails with a radial crack along the α-cut after heavy pinching of the wall and base depression. Pinching and base depression are always observed to occur in conjunction with tearing or to eventually lead to tearing. Therefore, they are included in the tearing label in Fig. 13. The achieved forming heights are defined as the final wall profile lengths L_f including the filleted corner; for asymmetric parts, the minimum forming height around the part is quoted. The graph shows that the forming height increases as S' increases, and decrease as ψ increases. This is because in an asymmetric part the minimum forming height is found along the β-cut, where $\kappa = \kappa_{\min}$. For the shapes selected in this study, $\kappa_{\min}$ decreases as ψ increases, so the minimum forming height around the part decreases with ψ. This effect is lessened at lower spinning ratios, because the local spinning ratios along the β-cut in each asymmetric part get closer together. The spinning ratios achieved before failure are somewhat lower than that achieved by Sugita and Arai (2015). This can be attributed the lower ratio between sheet thickness t_0 and mandrel diameter d' used in this study, which lowers the achievable spinning ratio (Lange, 1985).

Contrary to expectations, Fig. 13 reveals that the occurrence of failure in asymmetric spun parts is only weakly influenced by the planform asymmetry. Although our hypothesis was that the higher strains caused by the increased local curvature will be the foremost cause of tearing, the tendency of elliptical parts to tear earlier than square parts reveals that other, more dominant mechanisms are at play. In light of these results, control trials were performed to check for the effect of material anisotropy, which is a property of the cold rolled material from which the blanks were cut. Rolling reduces the thickness of sheet metal along a certain direction, elongating the grains in the microstructure; thus, the sheet is primed to undergo higher thickness reduction along the rolling direction. In the matrix of trials, the rolling direction was always aligned with the major axis of elliptical parts (thus, with the α-cut) and with the sides of the square parts (thus, with the β-cut). Therefore, two control trials were performed: an elliptical part with $\psi = 0.6$, $S' = 1.40$, and rolling direction aligned with the β-cut; and a square part with $\psi = 1.3$, $S' = 1.40$, and rolling direction aligned with the α-cut. The results are shown in Fig. 14: neither of the two parts failed. This means, on the one hand, that a circular, elliptical and square part all present the same formability in spinning if the alignment with the rolling direction is chosen appropriately; on the other hand, it means that the square part presents better formability than the elliptical one regardless of the rolling direction alignment.

5. Discussion: roller forces, thinning and shape error

The results of the matrix of trials show that our hypothesis was incorrect: all parts fail at very similar spinning ratios regardless of planform asymmetry. In this section, the results obtained from measurements of roller forces, thickness profiles and shape error are analysed and compared with the literature as the basis for potential explanations for the observed trends.

5.1. The roller forces during the process

Analysing how the measured roller forces change with the degree of asymmetry and with the spinning ratio can be helpful to explain trends in the occurrence of tearing. As reported by Polyblank and Allwood (2015), higher tool forces lead to higher thinning, which eventually

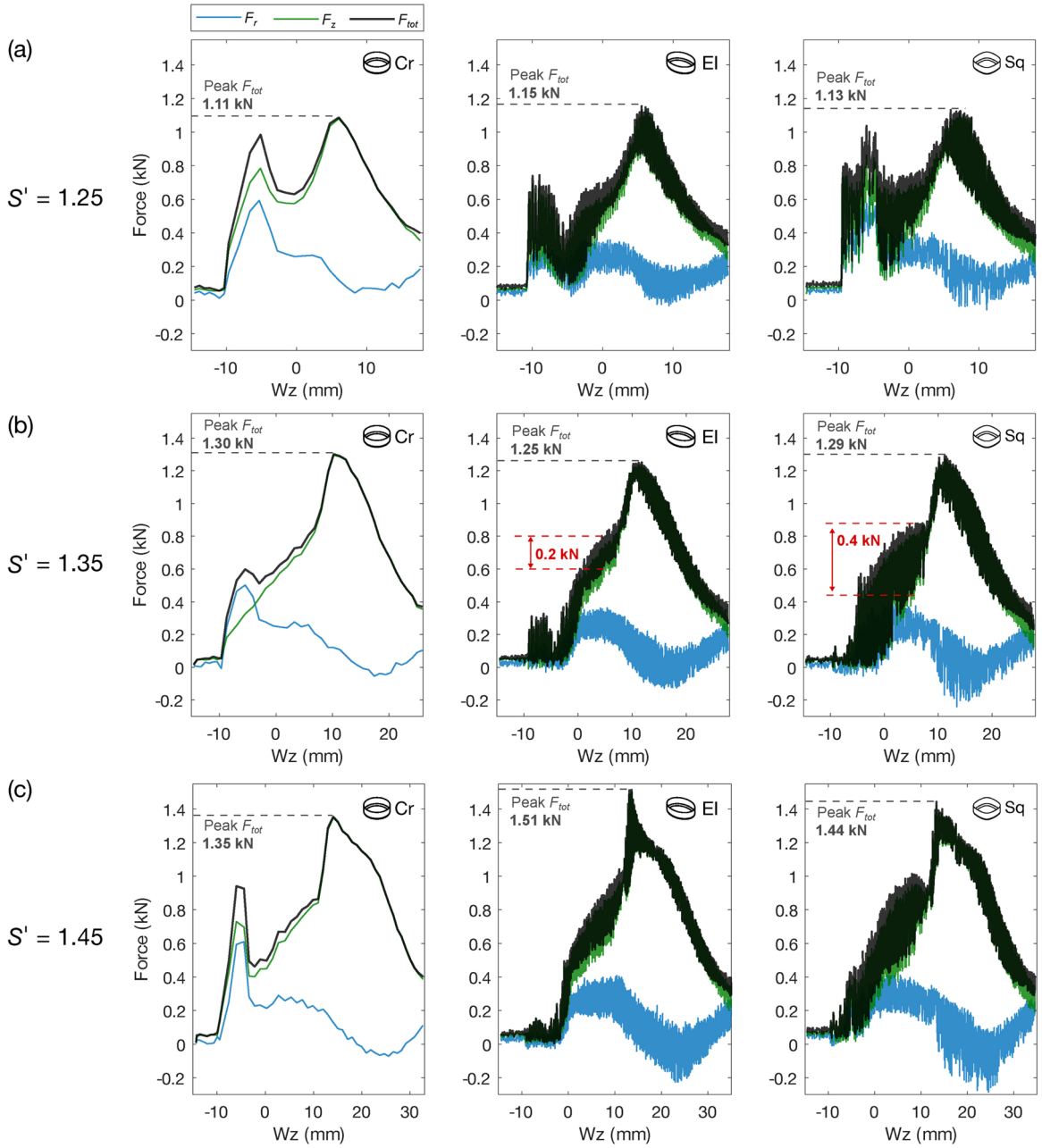

Fig. 15. Axial, radial and total roller forces measured on the WRol during Pass 4 for the three geometries a circular (Cr), elliptical (El) and square (Sq) part at (a) $S' = 1.25$, (b) at $S' = 1.35$, and (c) $S' = 1.45$. The forces are plotted against the WRol axial position Wz, and the peak total force reached in each trial is shown. The largest oscillations in force for the elliptical and square part are also highlighted in (b).

leads to tearing. During all trials performed in the study, the radial force F_r and axial force F_z on the WRol were measured, but comparing the full force history in all trials would require the analysis of an unwieldy quantity of data. Therefore, a key force measure for each trial must be identified. To do so, we note that the axial force component F_z dominates the overall roller force in spinning (Watson et al., 2015). Moreover, the results of all trials performed in this study showed that the highest WRol force is reached during Pass 4. The peak force reached during this pass should therefore allow us to compare all trials using a simple measure. Thus, in Fig. 15 we present the radial, axial and total WRol forces (F_r, F_z, F_{tot}) measured during Pass 4 for three key shapes (Cr, El1 and Sq1) at three increasing spinning ratios. Fig. 15 shows that the peak forces recorded at the same spinning ratio are very similar for the three part geometries, while they increase sharply as the spinning ratio increases. This agrees with the trend observed in the investigation of the forming limits (see Fig. 13): failure by tearing tends to occur at the same spinning ratio for all target geometries, because a higher force is required to form the workpiece flange and thinning in the part becomes more severe. Fig. 15 also reveals that both components of the WRol force oscillate significantly in the ellipse and square spinning. Taking the parts at $S' = 1.35$ in Fig. 15(b) as an example, we observe oscillations of amplitude up to 0.2 kN for the elliptical part and 0.4 kN for the square part. Compared with a peak force of 1.2–1.3 kN, this corresponds to a 16% oscillation for the elliptical and 30% oscillation for the square part.

To gain an insight into the pattern of force oscillation for the asymmetric parts, Fig. 16 presents the axial component of the WRol force F_z during one spindle revolution in Pass 4, for the three parts at $S' = 1.35$. For both the elliptical and square part, the force is highest in correspondence of the α-cut (high curvature, red points in Fig. 16), and

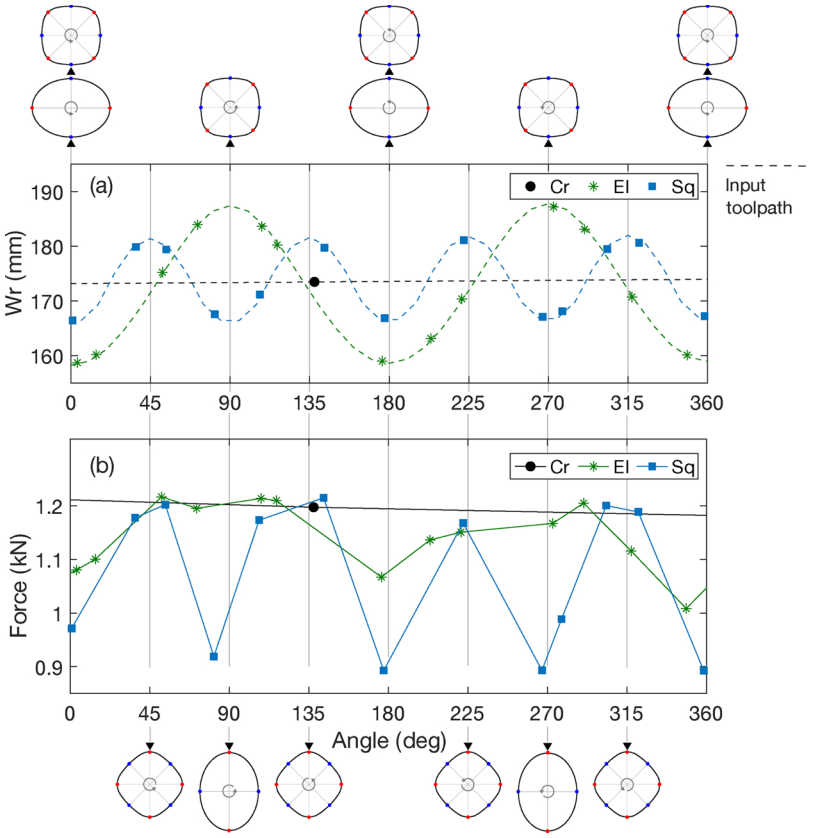

Fig. 16. (a) Measured radial WRol coordinate Wr plotted against rotation angle in one spindle revolution during Pass 4 for Cr, El1 and Sq1 at $S' = 1.35$. (b) Measured axial force F_z in the same spindle revolution. For both the elliptical and square parts, the lowest Wr corresponds to the β-cut while the highest Wr corresponds to the α-cut.

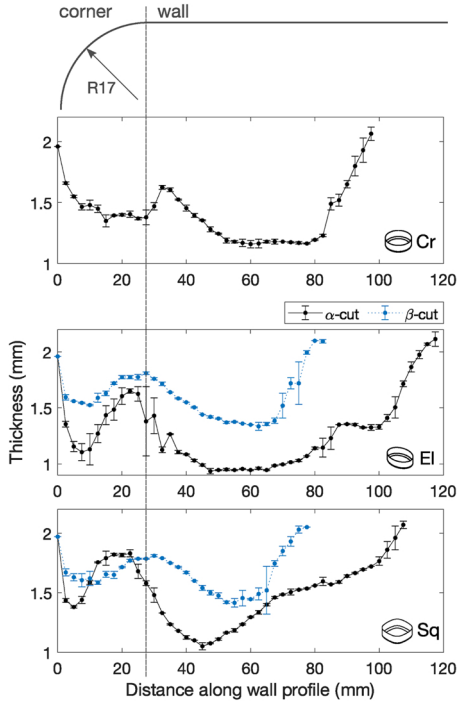

Fig. 17. Radial thickness profiles of in the circular (Cr), elliptical (El) and square (Sq) parts at $S' = 1.35$. The corner radius of is given by the 15 mm filleted corner radius plus the nominal thickness $t_0 = 2$ mm of the sheet. For each point in each profile, two measurements are taken and averaged: the error bars show the difference between the two measurements.

lowest in correspondence of the β-cut (low curvature, blue points in Fig. 16). This finding is consistent with the observation that tearing always occurred along the α-cut in the parts. However, to establish a clearer relationship between force, thinning and tearing, the pattern of thinning in the successful parts should also be considered and compared with the force. The next section will present the results obtained from measurements of thinning and shape error, it will show how they vary with curvature, and it will compare the trends with the force results.

5.2. *The influence of curvature on thinning and shape error*

As reviewed in Section 2.2, no consensus has been reached on the relationship between thinning and curvature in asymmetric spinning. To contribute to the available knowledge in this area, the results of measurements of workpiece thickness in the spun parts is reported here. The same parts are chosen for analysis as those of Fig. 16: a circular, an elliptical (El1) and a square (Sq1) part at the same spinning ratio of 1.35. The radial thickness profiles for these parts are shown in Fig. 17. For the asymmetric parts, the wall profiles along the α-cut and the β-cut are chosen for measurement; the former is longer because of earing. Three observations can be made. Firstly, all parts show a double dip in thickness occurring roughly in the middle the part's corner and in the middle of the wall, similar to the results reported by Shimizu (2010). Secondly, the highest radial thickness reduction is observed in the middle of the wall for all geometries, but in the elliptical part the corner along the α-cut shows significantly greater thickness reduction: this is in line with the results shown in the forming limit graphs, in which elliptical parts were observed to fail earlier than others with a crack appearing exactly in that area of the workpiece. Finally, the α-cut in asymmetric parts consistently shows higher thinning than the β-cut, both for the elliptical and square part. This finding is in line with the roller force measurements. It also agrees with the results obtained experimentally by Shimizu (2010) and Gao et al. (1999), while it contrasts with those obtained numerically by Cheng et al. (2013) and

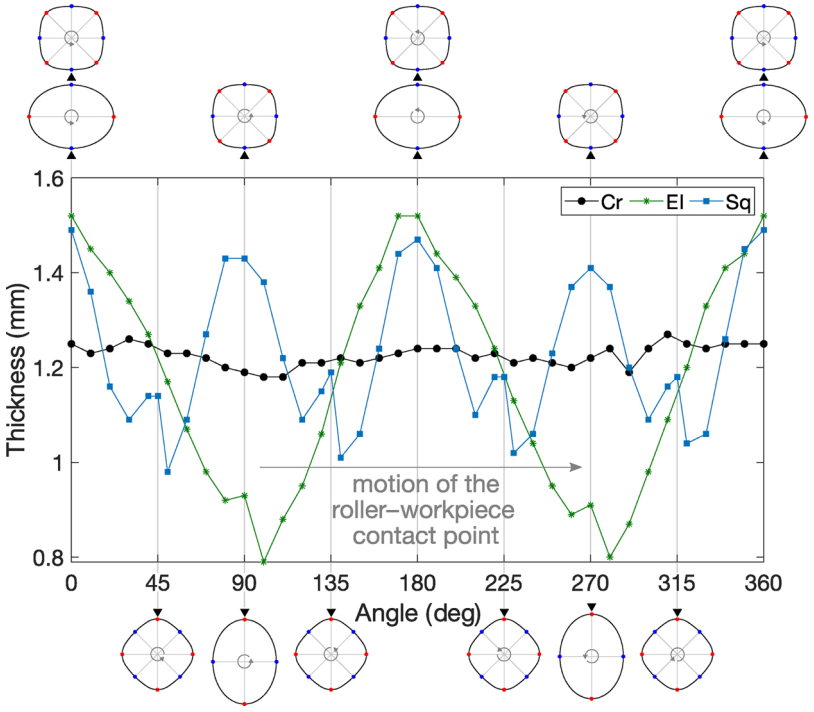

Fig. 18. Circumferential thickness profile of the circular (Cr), elliptical (El) and square (Sq) parts at $S' = 1.35$, taken at the same distance along the wall profile (50 mm).

experimentally by Sugita and Arai (2015).

The multi-pass spinning process performed by Sugita and Arai (2015) is the closest to the one presented in this study; therefore, the discrepancy in the results demands further analysis. To shed some more light on the issue, circumferential thickness profiles are also measured, and the results are shown in Fig. 18. Two key observations can be made. Firstly, the variation in thickness for the circular part is limited, while the variation in the elliptical and square part is very significant; this variation mirrors that of the force, and it confirms that higher force leads to higher thickness reduction. The elliptical part shows the greatest absolute thickness reduction, even though the variation in planform curvature is lower than in the square. This further discredits the idea that the only determinant of thinning in spinning is curvature. Secondly, the point of greatest thickness reduction for both asymmetric parts is offset from the α point (where $\kappa = \kappa_{max}$): it is found just after that point in the motion direction of the roller–workpiece contact point during the process. Because of the pinching effect previously shown, there is local thickening in the wall profile along the α-cut. The planform of the square cup spun by Sugita and Arai (2015) had corners with significantly higher curvature than the ones considered in this study; the thickening they observe along these corners could be explained as a pinching effect brought to its limits. The reason why the point of greatest reduction in Fig. 18 is found just after the and not at the α-point is unclear; a hypothesis is that surface shearing effects are at play due to the friction between the rollers and the workpiece as the rollers moves in and out radially in a single spindle revolution.

To complete the analysis, the workpiece wall profiles as measured by the laser profile scanner at the end of trials are presented in Fig. 19 for all three target geometries. Once again, the α and β-cuts are chosen for measurement in the elliptical and square parts. During the process, forming is interrupted once the maximum achievable height along the β-cut is reached, so that measured wall profiles along α-cut show ears with an angle in the range of 50–55° (see Fig. 22 in the Appendix). Significant springback is observable in the circular part and along the β-cut of the asymmetric parts; moreover, a bump in the measured profile can be seen just after the part's corner. The wall profile along the α-cut of the asymmetric parts is much closer to the target, because the tighter curvature hinders springback. In the case of the square part, base depression is evident along the α-cut and causes deviations in shape near the part's corner.

To obtain an overall view of the influence of planform curvature over the outcomes of a spinning process, the wall profile shape measurements are combined with the thickness measurements. Both shape and radial thickness profiles are measured for the successful trials presented in Fig 13 (i.e. all five target geometries up to $S' = 1.35$). This requires one set of measurements for each circular part, and two for each asymmetric part (along the α and the β-cuts). Each cut is associated to a local curvature κ in the planform: a single curvature for the circular part and two curvatures each for the asymmetric parts, as listed in Table 1. The mean shape error and the mean thickness reduction for all cuts are computed and related to the local planform curvature κ: Fig. 20 presents the results of this analysis. Two key conclusions can be drawn from the two mirrored plots. Firstly, the thickness reduction and the shape error do not scale monotonically with curvature: there is a peak in correspondence of the α-cuts of the two elliptical parts. Thus, it is confirmed that curvature alone cannot predict thinning nor shape error. Secondly, there appears to be an inverse relationship between thickness reduction and shape error, suggesting that a fundamental compromise exists between thickness retention and accuracy around an asymmetric spun part. This finding agrees with the results reported both by Amano and Tamura (1984) and Gao et al. (1999), who found a better geometrical accuracy of the product along the major axis of their elliptical parts, and lower thinning along the minor axis. The dependence of thinning and shape error on spinning ratio is more nuanced: for the β-cuts and for the circular part, higher thinning and shape error result from a higher spinning ratio; but for the α-cuts this relationship is not as clear, and sometimes completely inverted.

6. Conclusions

This paper has presented a rigorous methodology to perform asymmetric mandrel-free spinning and has demonstrated its successful application to spin circular, elliptical and square parts with no dedicated tooling. The hypothesis that increasing the degree of asymmetry

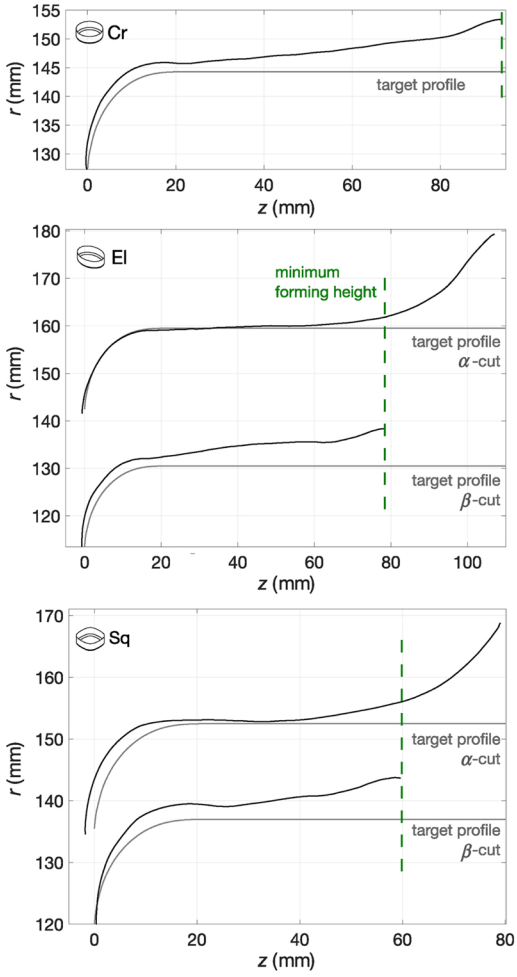

Fig. 19. Measured wall profiles compared to target wall profiles for the circular (Cr), elliptical (El) and square (Sq) geometries. Due to earing, the forming height varies around asymmetric parts; the minimum forming height, occurring along the β-cut, is indicated in the plots.

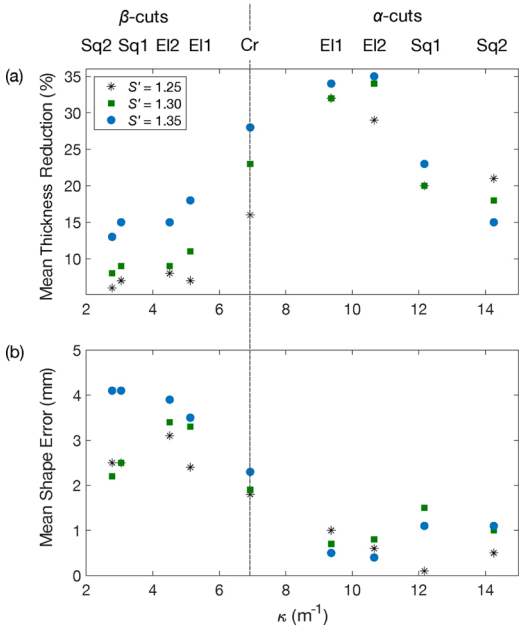

Fig. 20. (a) Mean thickness reduction and (b) mean shape error measured along the wall profiles of the five geometries investigated, plotted as a function of planform local curvature κ for three values of S'.

of the target part reduces the formability in multi-pass spinning was tested. The following conclusions can be drawn from the results:

1. In asymmetric spun parts, material accumulates in the areas of high planform curvature, causing earing and an uneven forming height. The difference in height is larger when the range of curvatures in the planform is larger. Future work could optimise the design of blanks to achieve uniform height for any target part.
2. In addition to the commonly encountered failure modes of wrinkling and tearing, asymmetric parts spun by mandrel-free spinning show a pinching effect along the profile of highest planform curvature and subsequent base depression. This occurs because of the lack of sufficient internal support to the workpiece, which is usually provided by the mandrel in conventional spinning.
3. The trend in the roller forces throughout the process is very similar for all target geometries at the same spinning ratio, but the peak force increases sharply with increasing spinning ratio. Oscillations of amplitude up to 17% of the peak force are observed in the elliptical parts, and up to 30% in the square parts; the highest force in individual spindle revolutions is measured where the curvature is highest, and the lowest force where the curvature is lowest.
4. Thinning in the part is higher in areas with high planform curvature than in areas with low planform curvature for all asymmetric parts studied. The greatest thickness reduction occurs just after the point of max curvature around the part, in the direction of motion of the roller–workpiece contact point. Shape error in the part follows an inverse trend: it is higher along the wall profiles with lowest curvature than along the profile with highest curvature. The results across different asymmetric shapes show that there is a compromise between thinning and shape error: the higher the former, the lower the latter, and vice versa.
5. The degree of asymmetry of the target part, measured as the range of curvature in the planform, only weakly influences formability in mandrel-free spinning; in fact, if material anisotropy is exploited, there is no reduction in the achievable spinning ratio for an elliptical and a square part compared to a circular part. This points to the great potential for the technique to spin a variety of geometries flexibly without sacrificing the achievable part height.
6. Other process and part parameters may influence the formability of asymmetric parts. In this study, the design of the blank and toolpath were fixed, but future work may explore how to optimise these process parameters; moreover, other part features such as negative curvature in the planform and more complex wall profiles are likely to affect the achievable forming height.

Acknowledgements

IMR is supported by a Doctoral Training Partnership (DTP) studentship provided by the UK's Engineering and Physical Sciences Research Council (EPSRC). CJC and JMA are supported by EPSRC grant EP/K018108/1. EGL is supported by EPSRC grant EP/S515760/1. EGL also acknowledges support from an Innovate UK project (FELDSPAR) and earlier funding from Nissan Motor Co., Ltd.

Appendix A. Motion control and measurement equipment

The two rollers can move on a plane in the radial (r) and axial (z) directions. Each axis is actuated by a servomotor with a ball-screw. The spindle is also actuated using a servomotor. The machine is controlled using a National Instruments CompactRIO-based real-time system. Motion applications are programmed using LabVIEW and the SoftMotion module. Synchronisation of all the machine axes is achieved by organising them in coordinates and using a contour move type. The inputs for the motion command are a set of coordinates for the WRol, BRol and spindle to follow, together with a time interval between successive points. The SoftMotion trajectory generation engine ensures that all axes reach the commanded position at the same time, thus guaranteeing synchronisation. A Catmull–Rom spline is selected for the trajectory generation because, as opposed to a Cubic B Spline, it ensures that the trajectory passes through all points commanded. Typical runtimes for a single toolpass in asymmetric spinning are of around 5 min. The speed of the process is limited by the acceleration of the servomotors in the r-direction.

Three key quantities are measured from the experiments: roller forces, part thickness and workpiece shape. Forces are measured using loadcells installed on the WRol in the r and z-direction. Thickness is measured using an Elcometer ultrasonic thickness gauge with a sensitivity of 0.01 mm. Thickness profiles are measured both radially along the meridian of the workpiece (i.e. its wall profile) and circumferentially around the perimeter of the planform. Workpiece shape and shape errors are measured using an Acuity AP620 profile measurement scanner, which can record the workpiece wall profile both during and after the trial (Fig. 21). Shape error measures are obtained by comparing the recorded wall profile of the workpiece with the target wall profile, using the methods employed by Polyblank et al. (2014). In the case of asymmetric shapes, only the wall profiles whose surface normals lie in the plane of the laser line are measured.

To give an idea of the progress of forming during an example trial, Fig. 22 shows videoframes of the process at the start and at the end, as well as during two intermediate stages. Pass 4 is part of the first stage of the process, in which the workpiece flange is formed from flat to 45° using rotational passes (see Fig. 9); Pass 12 is part of the second stage of the process, in which toolpasses in translational sequence bring a portion of the workpiece to its final position on the would-be mandrel, and move the half-formed flange forward in the z-direction.

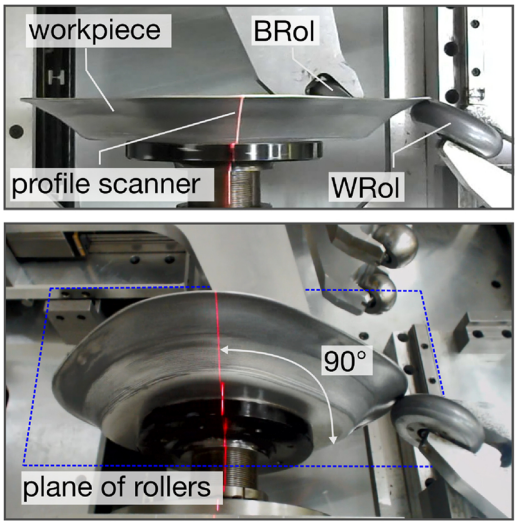

Fig. 21. Wall profile measurement using a laser profile scanner, which records the shape of the workpiece at 90° to the plane of the rollers.

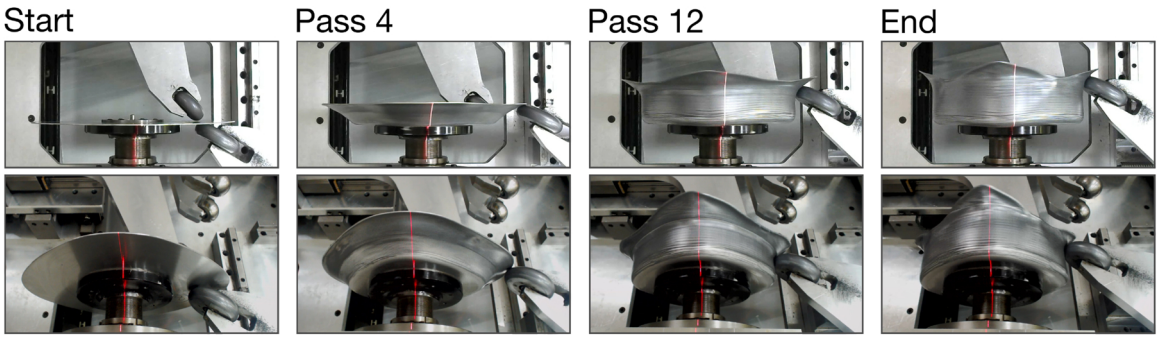

Fig. 22. Video-frames of an asymmetric spinning trial, as seen from above and behind the workpiece, showing the progress of forming for a square part.

Appendix B. Toolpath generation

Here, the calculations required to generate a toolpath with the correct roller–workpiece conditions are described. The starting point is a model of the target part, designed using CAD software (Solidworks is used in this study). The CAD model is meshed using triangular elements. The mesh is represented in the usual way with a connectivity matrix and an $q \times 3$ coordinate matrix $\mathbf{C} = [\mathbf{x} \quad \mathbf{y} \quad \mathbf{z}]$, where q is the number of nodes and $\mathbf{x}$, $\mathbf{y}$, $\mathbf{z}$ are q-tuples representing components of standard Cartesian coordinates. In addition, for all nodes, the Cartesian components of the unit normal vectors to the surface are calculated and are represented here by the $q \times 3$ matrix $\mathbf{N} = [\mathbf{n}_x \quad \mathbf{n}_y \quad \mathbf{n}_z]$. Then, for every tool pass $i = 1, \ldots, k$, the mesh of the

target part is offset according to the equations:

$$[\mathbf{x}_i \quad \mathbf{y}_i] = [\mathbf{x} \quad \mathbf{y}] + (m_i \mathbf{z}^{n_i} + t_0)[\mathbf{n}_x \quad \mathbf{n}_y] \tag{7}$$

and

$$\mathbf{C}_i = [\mathbf{x}_i \quad \mathbf{y}_i \quad \mathbf{z}] \tag{8}$$

where m and n are parameters input by the user to define the toolpass geometry. The target shape offset is a function of its height and the two parameters m and n. Only the portion of the target part which undergoes deformation from a flat blank is transformed; therefore, the base is excluded.

Once the intermediate mandrel surface is obtained, two parameters are defined: the feed ratio F, which determines the extent of motion along the slope of the surface in a single spindle revolution, and the number of points P at which the roller position is to be calculated in each revolution. At each point, the correct location of the roller centre (x_0, y_0, z_0) is calculated as follows. Firstly, the normals at all vertices of the mesh's triangular elements are calculated. Then, a number of points on the surface of the intermediate mandrel are selected near and around the current z_0. These points are used to define an interpolant, which is used to produce an array of points on the surface at z_0. For each point, the normal is found by interpolating between the normals of the three closest points on the original mesh. Once the normals are obtained, they are extended by a distance equal to the roller nose radius r_n. The resulting locus represents all possible locations of the nose profile, which is a circle. This circle is the intersection between a sphere centred at (x_0, y_0, z_0) and a plane inclined by θ with respect to the x-axis. The equation for the sphere is:

$$(x - x_0)^2 + (y - y_0)^2 + (z - z_0)^2 = (r_{\text{rol}} - r_n)^2 \tag{9}$$

where r_{rol} is the total roller radius. The equation of the plane is:

$$c_x(x - x_0) + c_y(y - y_0) + c_z(z - z_0) = 0 \tag{10}$$

Based on a angle θ between the plane passing through the middle of the roller and the x-axis:

$$[c_x, c_y, c_z] = [\sin(\theta), 0, \cos(\theta)] \tag{11}$$

It is also known that the roller centre lies on the xz-plane and hence $y_0 = 0$. From the equations above:

$$z_0 = z + \frac{c_x}{c_z}(x - x_0) \tag{12}$$

$$x_0 = x \pm \sqrt{\frac{(r_{\text{rol}} - r_n)^2 - y^2}{1 + (c_x^2/c_z^2)}} \tag{13}$$

This locus gives many possible roller centre locations: the one that maximises the distance between the roller centre and the candidate contact point is selected. This must be the correct location of the roller. If any other point is chosen, the roller will penetrate the mandrel surface. For the BRol, the normals are made to point inwards and the second solution for x_0 is chosen.

References

Ahmed, K.I., Gadala, M.S., El-Sebaie, M.G., 2015. Deep spinning of sheet metals. Int. J. Mach. Tools Manuf. 97, 72–85. https://doi.org/10.1016/j.ijmachtools.2015.07.005.

Amano, T., Tamura, K., 1984. Study of an elliptical cone spinning by the trial equipment. In: Proceedings of the 3rd International Conference on Rotary Metalworking Processes. IFS (Publ) Ltd.. pp. 213–224.

Arai, H., 2005. Robotic metal spinning – forming non-axisymmetric products using force control. J. Robot. Soc. Jpn. 24, 140–145. https://doi.org/10.1186/s13063.

Awiszus, B., Härtel, S., 2011. Numerical simulation of non-circular spinning: a rotationally non-symmetric spinning process. Prod. Eng. 5, 605–612. https://doi.org/10.1007/s11740-011-0335-9.

Awiszus, B., Meyer, F., 2005. Metal spinning of non-circular hollow parts. In: 8th International Conference on Technology of Plasticity. Italy, October 9–13.

Cheng, X.Q., Wu, X., Xia, Q., 2011. Research on thickness distribution of spun hollow part with four arc-typed cross-section. Proceedings of the 10th International Conference on Technology of Plasticity 560–563.

Cheng, X.Q., Xia, Q., Lai, Z.Y., 2013. Investigation on stress and strain distributions of hollow-part with triangular cross-section by spinning. Int. J. Mater. Prod. Technol. 47, 162–174.

Cooper, D.R., Rossie, K.E., Gutowski, T.G., 2016. An environmental and cost analysis of stamping sheet metal parts. J. Manuf. Sci. Eng. 139, 041012. https://doi.org/10.1115/1.4034670.

Gao, X.c., Kang, D.c., Meng, X.f., Wu, H.J., 1999. Experimental research on a new technology – ellipse spinning. J. Mater. Process. Technol. 94, 197–200.

Härtel, S., Laue, R., 2016. An optimization approach in non-circular spinning. J. Mater. Proc. Technol. 229, 417–430. https://doi.org/10.1016/j.jmatprotec.2015.09.003.

Hayama, M., Kudo, H., Shinokura, T., 1970. Study of the pass schedule in conventional simple spinning. Bull. JSME 13, 1358–1365. https://doi.org/10.1299/jsme1958.13.1358.

Jia, Z., Xu, Q., Han, Z., Peng, W.F., 2015. Precision forming of the straight edge of square section by die-less spinning. J. Manuf. Sci. Eng. 138, 011006. https://doi.org/10.1115/1.4030303.

Kawai, K., Yang, L., Kudo, H., 2001. A flexible shear spinning of truncated conical shells with a general-purpose mandrel. J. Mater. Process. Technol. 113, 28–33.

Handbook of Metal Forming. In: Lange, K. (Ed.), .

Music, O., Allwood, J.M., 2011a. Flexible asymmetric spinning. CIRP Ann. – Manuf. Technol. 60, 319–322.

Music, O., Allwood, J.M., 2011b. Tool-path design for metal spinning. Proceedings of the 10th International Conference on Technology of Plasticity 542–547.

Music, O., Allwood, J.M., Kawai, K., 2010. A review of the mechanics of metal spinning. J. Mater. Process. Technol. 210, 3–23. https://doi.org/10.1016/j.jmatprotec.2009.08.021.

Polyblank, J.A., Allwood, J.M., 2015. Parametric toolpath design in metal spinning. CIRP Ann. – Manuf. Technol. 64, 301–304. https://doi.org/10.1016/j.cirp.2015.04.077.

Polyblank, J.A., Allwood, J.M., Duncan, S.R., 2014. Closed-loop control of product properties in metal forming: a review and prospectus. J. Mater. Process. Technol. 214, 2333–2348. https://doi.org/10.1016/j.jmatprotec.2014.04.014.

Russo, I.M., Loukaides, E.G., 2017. Toolpath generation for asymmetric mandrel-free spinning. Procedia Eng. 207, 1707–1712. https://doi.org/10.1016/j.proeng.2017.10.926.

Shima, S., Kotera, H., Murakami, H., 1997. Development of flexible spin-forming method. J. JSTP 38, 814–818.

Shimizu, I., 2010. Asymmetric forming of aluminum sheets by synchronous spinning. J. Mater. Process. Technol. 210, 585–592. https://doi.org/10.1016/j.jmatprotec.2009.11.002.

Sugita, Y., Arai, H., 2015. Formability in synchronous multipass spinning using simple pass set. J. Mater. Process. Technol. 217, 336–344. https://doi.org/10.1016/j.jmatprotec.2014.11.017.

Watson, M., Long, H., 2014. Wrinkling failure mechanics in metal spinning. Procedia Eng. 81, 2391–2396. https://doi.org/10.1016/j.proeng.2014.10.339.

Watson, M., Long, H., Lu, B., 2015. Investigation of wrinkling failure mechanics in metal spinning by Box–Behnken design of experiments using finite element method. Int. J. Adv. Manuf. Technol. 78, 981–995. https://doi.org/10.1007/s00170-014-6694-6.

Xia, Q., Lai, Z., Zhan, X., Cheng, X., 2010. Research on spinning method of hollow part with triangle arc-type cross section based on profiling driving. Steel Res. Int. 81.

Xia, Q., Lai, Z.Y., Long, H., Cheng, X.Q., 2013. A study of the spinning force of hollow parts with triangular cross sections. Int. J. Adv. Manuf. Technol. 68, 2461–2470. https://doi.org/10.1007/s00170-013-4847-7.

Xia, Q., Shima, S., Kotera, H., Yasuhuku, D., 2005. A study of the one-path deep drawing spinning of cups. J. Mater. Process. Technol. 159, 397–400. https://doi.org/10.1016/j.jmatprotec.2004.05.027.